Central exclusive production of J/ψ and ψ(2S) mesons in pp collisions at s√=13 TeV

Aaij, R.; Adeva, B.; Adinolfi, M.; Ajaltouni, Z.; Akar, S.; Albrecht, J.; Alessio, F.; Dufour, L.; Mulder, M.; Onderwater, C. J. G.

Published in:
Journal of High Energy Physics

DOI:
10.1007/JHEP10(2018)167

Publication date:
2018

Published for SISSA by Springer

Received: June 15, 2018
Accepted: October 5, 2018
Published: October 26, 2018

Central exclusive production of J/ψ and $\psi(2S)$ mesons in pp collisions at $\sqrt{s} = 13$ TeV

The LHCb collaboration

E-mail: melody.ravonel@cern.ch

Abstract: Measurements are reported of the central exclusive production of J/ψ and $\psi(2S)$ mesons in pp collisions at a centre-of-mass energy of 13 TeV. Backgrounds are significantly reduced compared to previous measurements made at lower energies through the use of new forward shower counters. The products of the cross-sections and the branching fractions for the decays to dimuons, where both muons are within the pseudorapidity range $2.0 < \eta < 4.5$, are measured to be

$$\sigma_{J/\psi\to\mu^+\mu^-} = 435 \pm 18 \pm 11 \pm 17\,\text{pb}$$
$$\sigma_{\psi(2S)\to\mu^+\mu^-} = 11.1 \pm 1.1 \pm 0.3 \pm 0.4\,\text{pb}\,.$$

The first uncertainties are statistical, the second are systematic, and the third are due to the luminosity determination. The cross-sections are also measured differentially for meson rapidities between 2.0 and 4.5. Good agreement is observed with theoretical predictions. Photoproduction cross-sections are derived and compared to previous experiments, and a deviation from a pure power-law extrapolation of lower energy data is observed.

Keywords: Charm physics, Forward physics, Hadron-Hadron scattering (experiments), Particle and resonance production, Quarkonium

ArXiv ePrint: 1806.04079v2

https://doi.org/10.1007/JHEP10(2018)167

JHEP10(2018)167

Contents

1 Introduction 1

2 Detector, data samples and triggers 2

3 Event selection 3
- 3.1 HERSCHEL efficiency of selecting signal events 4
- 3.2 Purity of signal sample 6
- 3.3 Selection efficiency 8

4 Cross-section calculation 8

5 Systematic uncertainties 9

6 Results 11

7 Conclusions 14

A Additional material 17

The LHCb collaboration 22

1 Introduction

Central exclusive production (CEP) [1] of a vector meson in pp collisions is a diffractive process in which the protons remain intact and the meson is produced through the fusion of a photon and a colourless strongly coupled object, the so-called pomeron. For charmonia production, the cross-section can be predicted in perturbative quantum chromodynamics (QCD) and at the leading order (LO) is proportional to the square of the gluon parton distribution function (PDF), which ensures a steep rise in the photoproduction cross-section with the centre-of-mass energy of the photon-proton system, W. Therefore, measurements of CEP of the J/ψ and $\psi(2S)$ mesons provide not only a test of perturbative QCD but also probe the pomeron, and constrain the gluon PDF.

Elastic photoproduction of charmonia has been measured in fixed target experiments [2–4], in electron-proton [5–8], $p\bar{p}$ [9], and proton-lead collisions [10]. The LHCb collaboration has previously measured the CEP of the J/ψ and $\psi(2S)$ mesons in pp collisions at a centre-of-mass energy $\sqrt{s} = 7\,\text{TeV}$ [11]. In this paper, those results are extended to $\sqrt{s} = 13\,\text{TeV}$ and charmonia are measured up to $W = 2\,\text{TeV}$, the highest energy yet explored. This corresponds to probing the gluon PDF down to a fractional momentum of the proton, described by the Bjorken variable $x \approx 2 \times 10^{-6}$, a scale at which saturation effects may become visible [12].

JHEP10(2018)167

For diffractive processes, the dependence of the cross-section on the four-momentum transfer squared, t, is exponential with a slope b related to the transverse size of the interaction region. In Regge theory [13, 14], b varies with W according to $b = b_0 + 4\alpha' \log(W/W_0)$, where b_0 is the slope measured at an energy W_0. Measurements at HERA determined $\alpha' = 0.164 \pm 0.041\,\text{GeV}^{-2}$ with $b_0 = 4.63^{+0.07}_{-0.17}\,\text{GeV}^{-2}$ for J/ψ photoproduction at $W_0 = 90\,\text{GeV}$ [6]. In pp collisions at $\sqrt{s} = 7\,\text{TeV}$, LHCb measured $b = 5.70 \pm 0.11\,\text{GeV}^{-2}$ at an average value of $W = 750\,\text{GeV}$ [11]. According to Regge theory, a value of $b \approx 6.1\,\text{GeV}^{-2}$ is expected for J/ψ production in pp collisions at $\sqrt{s} = 13\,\text{TeV}$. In inelastic J/ψ production when proton dissociation occurs, the fall-off with t is more gradual. In contrast, the nonresonant ultraperipheral electromagnetic CEP of dimuons, produced through photon-photon fusion, peaks strongly at low t values. Therefore, the t dependence of the cross-section can be used to distinguish and study different production mechanisms.

This paper presents measurements of the cross-section for central exclusive production of charmonia with rapidity, y, between 2.0 and 4.5, and follows the methodology of the LHCb analysis at $\sqrt{s} = 7\,\text{TeV}$ [11]. Exclusive charmonium candidates are selected through their characteristic signature at a hadron collider: a pp interaction devoid of any activity save the charmonium that is reconstructed from its decay to two muons. The addition of new forward shower counters (HeRSCheL) [15] extends the pseudorapidity region in which particles can be vetoed and roughly halves the number of background events compared to the previous measurement.

The LHCb detector is outlined in section 2 while the data and selection criteria are described in section 3. The cross-section calculation is detailed in section 4 and systematic uncertainties are presented in section 5. The cross-section results for $pp \to pJ/\psi p$ and $pp \to p\psi(2S)p$ processes and derived photoproduction cross-sections for $\gamma p \to J/\psi p$ and $\gamma p \to \psi(2S)p$ are presented in section 6. Conclusions are given in section 7.

2 Detector, data samples and triggers

The LHCb detector [16, 17] is a single-arm forward spectrometer covering the pseudorapidity range $2 < \eta < 5$, designed for the study of particles containing b or c quarks. The detector includes a high-precision tracking system consisting of a silicon-strip vertex detector (VELO) surrounding the pp interaction region, a large-area silicon-strip detector located upstream of a dipole magnet with a bending power of about 4 Tm, and three stations of silicon-strip detectors and straw drift tubes placed downstream of the magnet. The tracking system provides a measurement of momentum, p, of charged particles with a relative uncertainty that varies from 0.5% at low momentum to 1.0% at 200 GeV.[1] Photons, electrons and hadrons are identified by a calorimeter system consisting of scintillating-pad (SPD) and preshower detectors, an electromagnetic calorimeter and a hadronic calorimeter. Muons are identified by a system composed of alternating layers of iron and multiwire proportional chambers [18].

The pseudorapidity coverage is extended by forward shower counters consisting of five planes of scintillators with three planes at 114, 19.7 and 7.5 m upstream of the interaction point, and two downstream at 20 and 114 m. At each location there are four quadrants

[1] Natural units with $c = 1$ are used throughout.

JHEP10(2018)167

of scintillators, whose information is recorded in every beam crossing by photomultiplier tubes, giving a total of 20 channels in HeRSCheL. These are calibrated using data taken without beams circulating at the end of each LHC fill. The pseudorapidity ranges covered by VELO and HeRSCheL are different. For VELO, the region is $-3.5 < \eta < -1.5$ and $2 < \eta < 5$, and for HeRSCheL, the region is $-10 < \eta < -5$ and $5 < \eta < 10$.

A data set corresponding to an integrated luminosity of $204 \pm 8\,\text{pb}^{-1}$ in pp collisions at $\sqrt{s} = 13\,\text{TeV}$ is used in this analysis. The average number of pp interactions per beam crossing, μ, is 1.1, thus in about half of visible interactions there is only a single pp collision and the CEP process is uncontaminated by pile-up. The online event selection is performed by a trigger that consists of two different stages. First, there is a hardware stage, which requires less than 30 deposits in the SPD and at least one muon with a transverse momentum, p_T, above 200 MeV. It is followed by a software stage, which applies a full event reconstruction and requires fewer than ten reconstructed tracks, at least one of which is identified as a muon.

Simulated signal events are generated using SuperCHIC v2.02 [19], where the J/ψ and $\psi(2S)$ mesons are transversely polarised. The J/ψ meson can also originate from exclusive χ_c decays, which are also generated with SuperCHIC, or from $\psi(2S)$ decays, which are handled by PYTHIA [20]. The LPAIR generator [21] is used to generate dimuons produced through the electromagnetic photon-photon fusion process. The interaction of the generated particles with the detector, and the detector response, are implemented using the Geant4 toolkit [22, 23] as described in ref. [24].

3 Event selection

The selection of candidate signal events is similar to that used in the previous LHCb analysis [11]. Two reconstructed muons are required in the region $2.0 < \eta < 4.5$, with an invariant mass within $\pm 65\,\text{MeV}$ of the known J/ψ or $\psi(2S)$ mass [25] and p_T^2 of the reconstructed meson below $0.8\,\text{GeV}^2$. The mass and p_T^2 requirements are both chosen to reject background while ensuring good signal efficiency, the evaluations of which are described in section 3.2 and 3.3.

Events with additional VELO tracks or photons with transverse energies above 200 MeV are vetoed. Events with significant deposits in HeRSCheL are removed. The HeRSCheL response is described using a variable χ^2_HRC that quantifies the activity above noise, taking account of correlations between the counters.

The invariant mass, M, of all candidates without the mass-window requirement applied is shown in figure 1. The data in the nonresonance regions (when $1500 < M < 2700\,\text{MeV}$, $3200 < M < 3500\,\text{MeV}$ and $3800 < M < 8000\,\text{MeV}$) are candidates for electromagnetic CEP dimuons produced by photon-photon fusion and constitute an important calibration sample. The p_T^2 distribution of these dimuons with and without the requirement on χ^2_HRC is shown in figure 2 and is significantly peaked towards low values due to the long-range electromagnetic interaction. The fraction of electromagnetic CEP events in this sample is determined from a fit to the p_T^2 distribution with two components: a signal shape taken from simulated events and an inelastic background modelled with the sum of two exponential functions.

JHEP10(2018)167

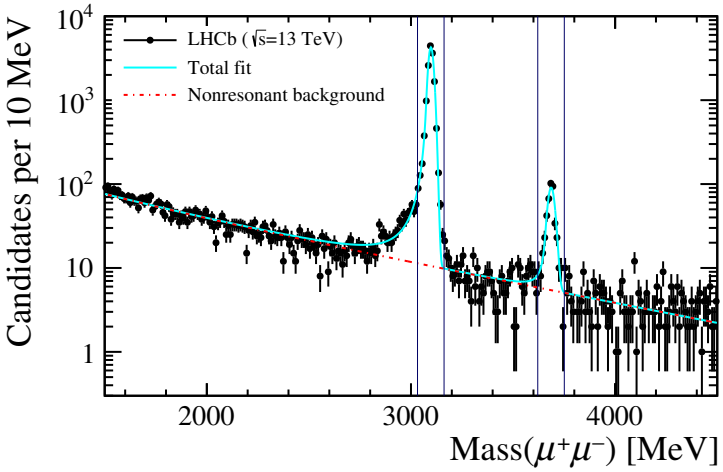

Figure 1. Invariant mass distribution of dimuon candidates. The J/ψ and $\psi(2S)$ mass windows of the signal regions are indicated by the vertical lines.

The power of HeRSCheL to discriminate CEP events can be seen in figure 3, which shows the distributions of $\chi^2_{\rm HRC}$ for three classes of low-multiplicity-triggered events. The first class is CEP-enriched dimuons: events in the nonresonant dimuon sample with $p_{\rm T}^2 < 0.01\,{\rm GeV}^2$, which has a purity of 97% for electromagnetic CEP events. The second class, inelastic-enriched J/ψ, applies the nominal J/ψ selections but requires $p_{\rm T}^2 > 1\,{\rm GeV}^2$, thus selecting inelastic events with proton dissociation. The third class consists of events with more than four tracks reconstructed. Figure 3 shows that CEP-enriched events have lower values of $\chi^2_{\rm HRC}$. To select exclusive J/ψ and $\psi(2S)$ candidates, it is required that $\log(\chi^2_{\rm HRC}) < 3.5$; this value is chosen in order to minimise the combined statistical and systematic uncertainty on the total cross-sections. After the event selections, there are 14 753 J/ψ signal candidates and 440 $\psi(2S)$ signal candidates remaining.

The estimation of the signal efficiency, $\epsilon_{\rm H}$, for the requirement $\log(\chi^2_{\rm HRC}) < 3.5$ is described in section 3.1. Using this, section 3.2 explains how the purity of the signal sample is estimated. The signal efficiency of all selection requirements is detailed in section 3.3.

3.1 HeRSCheL efficiency of selecting signal events

The efficiency for the veto on HeRSCheL activity is estimated from data using the nonresonant calibration sample. The fits to the $p_{\rm T}^2$ distributions in figure 2 give the numbers of electromagnetic CEP events with and without the HeRSCheL veto. The ratio of these gives the efficiency of the veto, which is determined to be $\epsilon_{\rm H} = 0.723 \pm 0.008$. The signal loss includes in particular a contribution from events where there is an additional primary interaction only seen in the HeRSCheL detector, as well as spill-over from previous collisions, electronic noise and calibration effects, as discussed in ref. [15]. This efficiency, measured using the nonresonant sample, is applicable to any CEP process, with the same veto, collected in this data-taking period.

JHEP10(2018)167

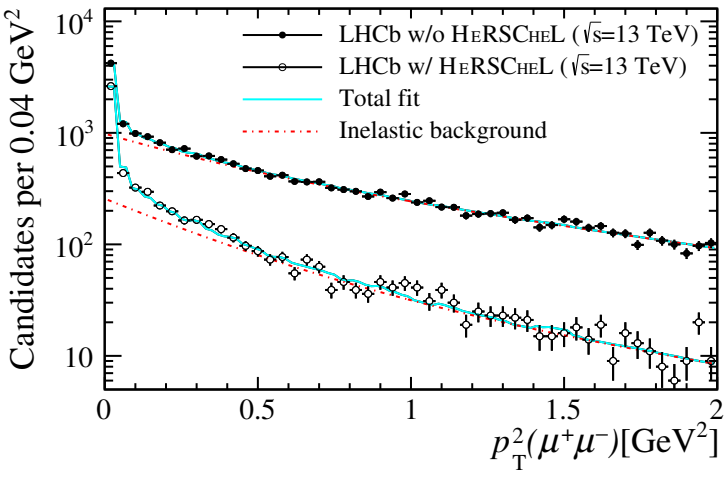

Figure 2. Transverse momentum squared for dimuons in the nonresonant region. The upper distributions are without any requirement on HERSCHEL: the lower are with the HERSCHEL veto applied. The total fit includes the electromagnetic CEP signal events as described by the LPAIR generator as well as the inelastic background.

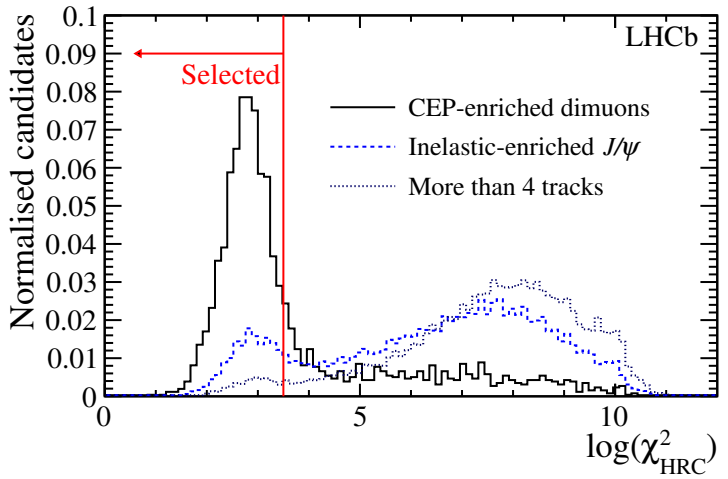

Figure 3. Distributions, normalised to unit area, of the logarithm of the discriminating variable $\chi^2_{\rm HRC}$ that is related to activity in HERSCHEL. The response to three classes of events, as described in the text, is shown. The selection requirement for the analysis is indicated by the red vertical line and the arrow.

JHEP10(2018)167

3.2 Purity of signal sample

Three background sources are considered: nonresonant dimuon production; feed-down of CEP $\chi_{cJ}(1P)$ or $\psi(2S)$ to J/ψ mesons and other undetected particles; and nonexclusive events where the proton dissociates but the remnants remain undetected.

The amount of nonresonant background is determined from the fit shown in figure 1, where the signals are modelled with two Crystal Ball functions [26] and the nonresonant background with the sum of two exponential functions. This background is estimated to contribute a fraction of 0.009 ± 0.001 to the J/ψ and 0.161 ± 0.018 to the $\psi(2S)$ samples.

The $\psi(2S)$ feed-down background in the J/ψ selection is determined using simulated events that have been normalised to have the same yield as the $\psi(2S) \to \mu^+\mu^-$ signal in data and is estimated to contribute a fraction 0.015 ± 0.001 to the J/ψ samples. The $\chi_{cJ}(1P)$ feed-down background is determined using a data calibration sample, which contains events that pass the nominal J/ψ selection, except instead of zero photons, it is required that there is exactly one reconstructed photon with a transverse energy above 200 MeV. The numbers of $\chi_{c0}(1P)$, $\chi_{c1}(1P)$, and $\chi_{c2}(1P)$ candidates in this calibration sample are determined from a fit to the invariant mass of the dimuon plus photon system. These are scaled by the ratio of J/ψ to $J/\psi + \gamma$ candidates in the corresponding simulated $\chi_{cJ}(1P)$ sample from which it is esimated that a fraction of 0.005 ± 0.001 of the J/ψ candidate sample is due to feed-down from $\chi_{c0}(1P)$ mesons, 0.002 ± 0.001 from $\chi_{c1}(1P)$ mesons, and 0.038 ± 0.002 from $\chi_{c2}(1P)$ mesons. The total feed-down ratio from $\psi(2S)$ and $\chi_{cJ}(1P)$ mesons is 0.060 ± 0.002, to be compared to 0.101 ± 0.009 in the previous analysis [11]: the addition of HeRSCheL suppresses events with proton dissociation, which are more numerous in the double-pomeron-exchange process that mediates $\chi_{cJ}(1P)$ production.

The fraction of nonexclusive events due to proton dissociation is determined through the p_{T}^2 distribution of the J/ψ and the $\psi(2S)$ candidates, after a background subtraction to remove contributions coming from the electromagnetic nonresonant and feed-down backgrounds. The electromagnetic component is shown in figure 2, while the feed-down shape is taken from the $J/\psi + \gamma$ calibration sample. The background-subtracted p_{T}^2 distribution consists of two remaining components: signal and proton dissociation background. Since $t \approx -p_{\mathrm{T}}^2$, approximately exponential distributions with different slopes are expected for each. In the previous analysis [11], each was modelled by an exponential function whose slope was a free parameter. The presence of the HeRSCheL detector however now allows these shapes to be determined from data, thus reducing the model dependence of the result.

The background subtracted distribution without HeRSCheL veto applied is split into two distributions: S_{H} if $\log(\chi^2_{\mathrm{HRC}}) < 3.5$ (corresponding to the signal selection), and $S_{\bar{\mathrm{H}}}$ otherwise. Since ϵ_{H} and $(1 - \epsilon_{\mathrm{H}})$ are the respective efficiencies for a CEP event to enter the distributions S_{H} and $S_{\bar{\mathrm{H}}}$, the distribution, $\beta = S_{\bar{\mathrm{H}}} - ((1 - \epsilon_{\mathrm{H}})/\epsilon_{\mathrm{H}})S_{\mathrm{H}}$, by construction has no contribution coming from exclusive events. The distribution for β approximates to the shape of the proton dissociation in the candidate distribution S_{H}, but is not exactly the same since the efficiency to veto nonexclusive events has a weak dependence on p_{T}^2. Consequently, the proton dissociation in the distribution S_{H} is estimated by scaling the distribution β by $f(p_{\mathrm{T}}^2) \equiv S_{\mathrm{H}}(p_{\mathrm{T}}^2)/\beta(p_{\mathrm{T}}^2)$.

JHEP10(2018)167

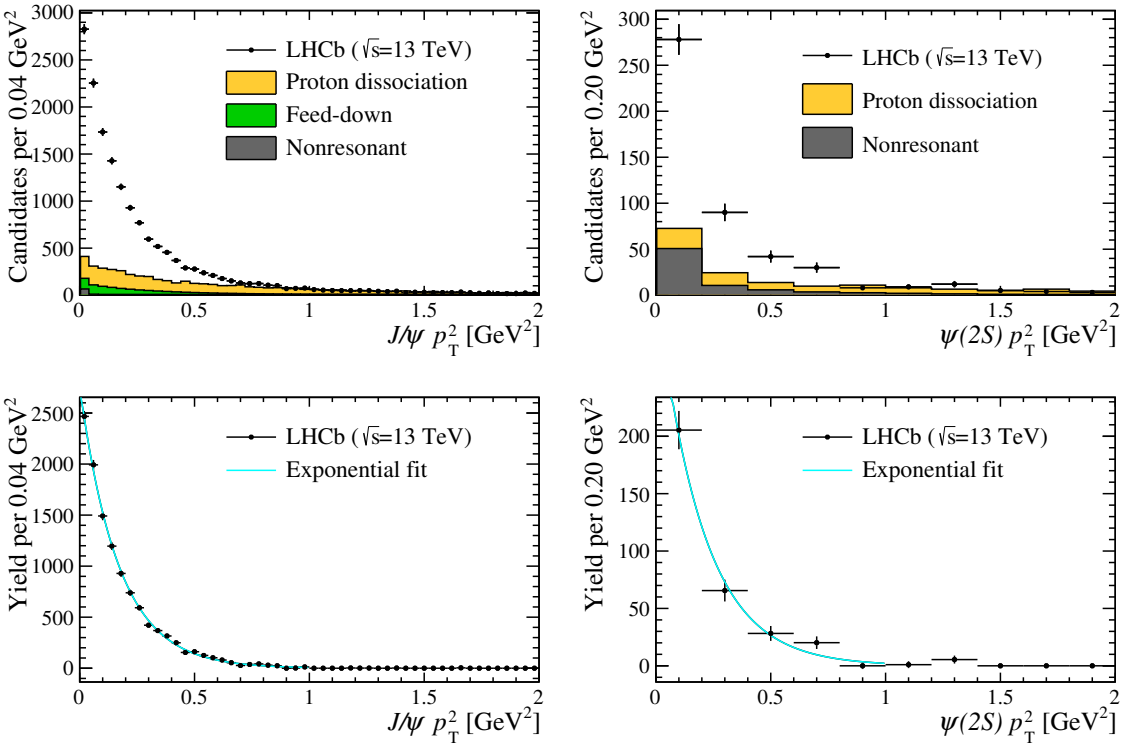

Figure 4. Top: transverse momentum squared distribution of (left) J/ψ and (right) $\psi(2S)$ candidates when data is below the HeRSCheL threshold. Bottom: CEP signal for the (left) J/ψ and (right) $\psi(2S)$ selections. The single exponential fit of the signal is shown by the curve superimposed on the data points.

The scale factor $f(p_T^2)$ is known from data for values of $p_T^2 \gtrsim 0.8\,\text{GeV}^2$, since there is little signal in this region as the signal distribution is expected to follow $\exp(-b_{\text{sig}} p_T^2)$ with $b_{\text{sig}} \approx 6\,\text{GeV}^{-2}$. An extrapolation of $f(p_T^2)$ is performed to the region $p_T^2 < 0.8\,\text{GeV}^2$ using functions which fit the data well in the region $p_T^2 > 0.8\,\text{GeV}^2$. The default is an exponential function for the J/ψ analysis and a constant for the $\psi(2S)$ analysis. A linear dependence is used to estimate the systematic uncertainty.

The p_T^2 candidate distributions in data with the estimated backgrounds superimposed are shown in the upper row of figure 4. The lower row shows the signal components after subtracting the proton dissociation background. These are fitted with a single exponential function, $\exp(-b_{\text{sig}} p_T^2)$, to test the hypothesis that the signal has this dependence. The J/ψ signal contribution is well described with $b_{\text{sig}} = 5.93 \pm 0.08\,\text{GeV}^{-2}$, consistent with extrapolations from previous pp measurements at 7 TeV and from H1 results [5, 11]. The corresponding slope, in the $\psi(2S)$ analysis, is $b_{\text{sig}} = 5.06 \pm 0.45\,\text{GeV}^{-2}$. Fits to the derived proton dissociation components show that these are also consistent with a single exponential.

In the region $0 < p_T^2 < 0.8\,\text{GeV}^2$, 0.175 ± 0.015 of the J/ψ candidate sample is estimated to be due to proton-dissociation events, while for the $\psi(2S)$ sample the contamination is estimated to be 0.11 ± 0.06. The uncertainties are statistical, and the correlation between

JHEP10(2018)167

the HeRSCheL efficiency and the proton-dissociation contamination is taken into account. The current analysis shows an approximate halving of the proton-dissociation background compared to the analysis at $\sqrt{s} = 7\,\text{TeV}$, due to the additional HeRSCheL veto. The overall purities are 0.755 ± 0.015 and 0.726 ± 0.061 for the J/ψ and $\psi(2S)$ selections, respectively.

3.3 Selection efficiency

The efficiency for selecting signal events is the product of the reconstruction efficiency, ϵ_{rec}, and selection efficiency, ϵ_{sel}. The reconstruction efficiency is the product of trigger, tracking, muon chamber acceptance and muon identification efficiencies. The acceptance is determined from simulation. The other quantities are determined from simulation and scaled using a data calibration sample. The trigger efficiency is calibrated through the fraction of events where both muons pass the trigger, in a sample collected with the requirement that at least one muon passes the trigger. The muon identification efficiency is calibrated using a sample enriched in J/ψ mesons that has been selected requiring a single identified muon. The tracking efficiency is calibrated using low-multiplicity events where the dimuon hardware was triggered by two objects having an absolute azimuthal angular difference close to π.

The efficiency for the selection requirements on the mass and transverse momentum of the J/ψ candidate, and the veto on additional tracks, photon activity, or HeRSCheL activity is obtained from data.

The fits to the mass distributions in figure 1 determine the fraction of signal inside the mass window and give a signal efficiency of 0.967 ± 0.002. No dependence on rapidity is found.

The efficiency for the requirement on the meson candidates that $p_{\text{T}}^2 < 0.8\,\text{GeV}^2$ is 0.993 ± 0.001 and is determined from the fitted slope to the signal components shown in figure 4 as described in the previous section. A small dependence on rapidity y is introduced through the Regge extrapolation of the exponential slope: $b = b_0 + 4\alpha' \log(W/W_0)$, where $W^2 = M_\psi e^y \sqrt{s}$.

The signal efficiency of vetoing events with additional VELO tracks or photons is obtained using the same technique described in section 3.1 to determine the HeRSCheL veto efficiency. When vetoing events with additional VELO tracks, no dependence on rapidity is found in simulation, while a slight dependence is observed for the photon veto, which is due to material effects in the detector whose density varies with rapidity. The shape of the rapidity dependence is taken from simulation and normalised to data. The efficiency of vetoing events with VELO tracks is determined to be 0.969 ± 0.004 and of vetoing events with photons is on average 0.983 ± 0.003.

4 Cross-section calculation

The products of the cross-sections and the branching fractions of the decays to two muons, $\sigma_{\psi \to \mu\mu}$, are measured differentially in ten equally spaced bins of J/ψ rapidity and three unequal bins of $\psi(2S)$ rapidity in the range $y \in (2.0, 4.5)$. The measurements are limited to the fiducial region where both muons have pseudorapidities between 2.0 and 4.5.

JHEP10(2018)167

The differential cross-section in each bin is

$$\frac{\mathrm{d}\sigma_{\psi\to\mu^+\mu^-}}{\mathrm{dy}}(2.0<\eta_\mu<4.5)=\frac{\mathcal{P}N}{\epsilon_{\mathrm{rec}}\epsilon_{\mathrm{sel}}\Delta y\epsilon_{\mathrm{single}}\mathcal{L}_{\mathrm{tot}}}, \tag{4.1}$$

and the total cross-section, summed over all bins, is also calculated. In eq. (4.1), N is the number of selected events, ϵ_{rec} and ϵ_{sel} are the efficiencies described in section 3.3, $\mathcal{P}$ is the purity given in section 3.2, Δy is the width of the rapidity bin, $\mathcal{L}_{\mathrm{tot}}$ is the integrated luminosity and $\epsilon_{\mathrm{single}}$ is the efficiency for selecting single interaction events, which accounts for the fact that the selection requirements reject signal events that are accompanied by a visible proton-proton interaction in the same beam crossing.

The number of visible pp interactions per beam crossing, v, is assumed to follow a Poisson distribution, $P(v)=\mu^v e^{-\mu}/v!$. The mean μ is determined from the fraction of beam crossings with no visible activity and is calculated over the data-taking period in roughly hour-long intervals. The probability that a signal event is not rejected due to the presence of another visible interaction is given by $P(0)$ and therefore $\epsilon_{\mathrm{single}}=e^{-\mu}$ which is equal to 0.3329 ± 0.0003. This value is about 40% higher than the corresponding one in the 7 TeV analysis. The lower number of pp interactions per beam crossing at $\sqrt{s}=13\,\mathrm{TeV}$ benefits the collection of CEP events. The integrated luminosity is evaluated as $204\pm8\,\mathrm{pb}^{-1}$ and is found from μ and a constant of proportionality that is measured in a dedicated calibration dataset [27].

5 Systematic uncertainties

Various sources of systematic uncertainties have been considered and are summarised in table 1 for the total cross-section. Excluding the uncertainty on the luminosity, they amount to 2.5% in the J/ψ and 2.7% in the $\psi(2S)$ cases.

The largest source of systematic uncertainty comes from the determination of the HeRSCheL efficiency. The fit to the p_{T}^2 distribution in figure 2 depends on assumptions made on the shape of the signal and background components. A systematic uncertainty is assessed firstly by changing the functional form of the background description, secondly by fitting only the tail of the distribution and extrapolating the result to the signal, and thirdly by using only the candidates in the first bin of the p_{T}^2 distribution where the signal dominates. The differences of each to the nominal fit are combined in quadrature which results in a systematic uncertainty of 1.7% on the total cross-section.

Since the same methodology is used to determine the efficiency for vetoing events with additional VELO tracks or photons, the associated systematic uncertainty is estimated with the same procedure. Since the simulation shows a dependence on rapidity for the efficiency due to the photon requirement, an additional uncertainty is added in quadrature in each rapidity bin, corresponding to the limited sample size of the simulation. This leads to a total systematic uncertainty of 0.2% on the total cross-section due to each veto requirement.

The systematic uncertainty on the efficiency of the mass-window requirement is obtained by repeating the fit shown in figure 1 with the mass peak and resolution fixed to the values of the simulation. The fit is also repeated by changing the background description to a single exponential function across the whole region. The biggest difference with the nominal fit between these two alternative fits is taken as the systematic uncertainty, which is 0.6% on the total cross-sections.

JHEP10(2018)167

Source	J/ψ analysis (%)	$\psi(2S)$ analysis (%)
HERSCHEL veto	1.7	1.7
2 VELO track	0.2	0.2
0 photon veto	0.2	0.2
Mass window	0.6	0.6
p_{T}^2 veto	0.3	0.3
Proton dissociation	0.7	0.7
Feed-down	0.7	-
Nonresonant	0.1	1.5
Tracking efficiency	0.7	0.7
Muon ID efficiency	0.4	0.4
Trigger efficiency	0.2	0.2
Total excluding luminosity	2.5	2.7
Luminosity	3.9	3.9

Table 1. Summary of relative systematic uncertainties on the total cross-section.

The uncertainty on the efficiency of selecting candidates with $p_{\mathrm{T}}^2 < 0.8\,\mathrm{GeV}^2$ is 0.3%. It is obtained by varying the signal shape from that shown in figure 4 to the one obtained by using the approach of the previous analysis [11] where the p_{T}^2 distribution is fitted with two exponential functions, one describing the proton dissociation and the other the signal shape. The slope and normalisations of each are free. The difference in efficiency between the two approaches is added in quadrature to the uncertainty coming from the propagation of the uncertainties on the parameters describing the Regge dependence that determines the rapidity dependence.

The proton-dissociation contamination depends on the extrapolation from the background-dominated high p_{T}^2 region to the signal-dominated low p_{T}^2 region. The corresponding systematic uncertainty is assigned by changing the form of the extrapolation function from the nominal exponential one to an alternative linear function, or fitting the p_{T}^2 distribution with two exponential functions to get the background contamination. The systematic uncertainty is the biggest difference between the nominal results and those from the two alternative approaches, and corresponds to 0.7% on the total cross-section.

The systematic uncertainty due to the feed-down contribution in the J/ψ analysis is assessed to be 0.7% on the total cross-section. It corresponds to the largest difference in the cross-section determination from a series of alternative fits to the $J/\psi + \gamma$ spectrum in which the photon energy scale, photon detection efficiency, invariant mass resolution, material interactions, and the $\psi(2S)$ contribution, are each varied by their estimated uncertainties.

An alternative estimate of the nonresonant background in figure 1 is performed by fitting a single exponential function between 1.5 and 2.5 GeV and extrapolating this into the signal region. This changes the total cross-section by 0.1% in the J/ψ analysis and 1.5% in the $\psi(2S)$ analysis. These values are taken as systematic uncertainties due to the nonresonant background.

JHEP10(2018)167

The reconstruction efficiency is taken from simulated events and calibrated using data. The technique depends on tagging a muon that fired the trigger and probing a partially reconstructed track that forms a J/ψ candidate. To assess the systematic uncertainty due to the method, this technique is applied to two simulated samples that have different tracking efficiencies. The resulting tracking efficiencies are compared after calibration using data. In a second test of the methodology, one simulated sample is taken as pseudodata and the other simulated sample applies the calibration procedure. The resulting efficiencies are compared to the true values in the pseudodata. The largest difference in each rapidity bin is assigned as a systematic uncertainty, which is assumed to be fully correlated between bins, and varies from 0.5% to 3.1% depending on the sample size. A systematic uncertainty on the method used in evaluating the muon identification and trigger efficiencies is assigned by comparing the derived values in simulation with truth, resulting in a 0.4% uncertainty on the total cross-section due to the muon identification, and 0.2% due to the trigger. The systematic uncertainty on the muon chamber acceptance is determined from the difference in the kinematic distributions in data and simulation, and its effect on the final reconstruction efficiency systematic uncertainty is negligible in all bins.

A bin migration uncertainty has been estimated using simulation to relate the reconstructed and true rapidity bin. The difference is smaller than 0.06% in all bins and so is considered negligible.

Most systematic uncertainties are assumed to be 100% correlated between rapidity bins except the photon-veto-shape systematic uncertainty, which is assumed to be independent between bins as it depends on the statistical precision of the simulation. As the determination of the sample purity depends on the HERSCHEL efficiency, these two quantitities are correlated. The correlation factors are determined in simulation, and the values are $\rho = -0.50$ and $\rho = -0.06$ for the J/ψ and $\psi(2S)$ selection, respectively. The lower statistical precision of the $\psi(2S)$ sample imposes less constraint on the proton dissociation scale factor $f(p_{\mathrm{T}}^2)$ and results in a smaller correlation. The total systematic uncertainties are given in table 1 taking account of the correlations.

6 Results

The product of the differential cross-sections and branching fractions to two muons, with both muons inside the fiducial acceptance $2.0 < \eta < 4.5$, are given per meson rapidity bin in tables 2 and 3 for J/ψ and $\psi(2S)$ mesons, respectively. The tables also present a summary of the numbers entering the cross-section calculation. The correlations between the statistical and systematic uncertainties in each bin are shown in tables 5 and 6 in the appendix. Summing these differential results leads to measurements of the product of the cross-sections and branching fractions, where both muons are within the fiducial region, $2.0 < \eta < 4.5$:

$$\sigma_{J/\psi\to\mu^+\mu^-}(2 < \eta < 4.5) = 435 \pm 18 \pm 11 \pm 17\,\mathrm{pb}$$
$$\sigma_{\psi(2S)\to\mu^+\mu^-}(2 < \eta < 4.5) = 11.1 \pm 1.1 \pm 0.3 \pm 0.4\,\mathrm{pb}\,.$$

The first uncertainties are statistical and include the uncertainties on the data-driven efficiencies and purities, the second are systematic, and the third are due to the luminosity determination.

JHEP10(2018)167

y bin	2.0−2.25	2.25−2.5	2.5−2.75	2.75−3.0	3.0−3.25
N	259	1022	1644	2204	2482
Stat. unc. (%)	6.2	3.1	2.5	2.1	2.0
$\epsilon_{\rm rec}$	0.410	0.525	0.555	0.565	0.563
Stat. unc. (%)	5.9	4.2	3.3	2.8	2.6
Syst. unc. (%)	3.1	0.8	1.7	1.0	0.5
$\epsilon_{\rm sel}$	0.636	0.643	0.650	0.655	0.663
Stat. unc. (%)	1.2	1.2	1.2	1.2	1.2
Syst. unc. (%)	2.5	2.0	2.0	1.9	1.9
Purity	0.760	0.759	0.751	0.758	0.764
Stat. unc. (%)	2.7	2.2	2.2	2.1	2.1
Syst. unc. (%)	1.0	1.0	1.0	1.0	1.0
$\mathrm{d}\sigma/\mathrm{d}y$(pb)	44	134	200	263	296
Stat. unc. (%)	9.2	6.0	5.0	4.5	4.3
Syst. unc. (%)	4.3	2.7	3.1	2.7	2.6
Lumi. unc. (%)	3.9	3.9	3.9	3.9	3.9

y bin	3.25−3.50	3.50−3.75	3.75−4.0	4.0−4.25	4.25−4.5
N	2522	2112	1433	829	246
Stat. unc. (%)	2.0	2.2	2.6	3.5	6.4
$\epsilon_{\rm rec}$	0.587	0.599	0.588	0.551	0.518
Stat. unc. (%)	2.5	2.6	2.8	3.3	4.1
Syst. unc. (%)	0.6	0.6	0.5	0.8	0.9
$\epsilon_{\rm sel}$	0.665	0.670	0.670	0.676	0.667
Stat. unc. (%)	1.2	1.2	1.2	1.2	1.2
Syst. unc. (%)	1.9	1.9	1.9	1.9	2.0
Purity	0.763	0.749	0.748	0.732	0.738
Stat. unc. (%)	2.1	2.1	2.2	2.4	3.1
Syst. unc. (%)	1.0	1.0	1.0	1.0	1.0
$\mathrm{d}\sigma/\mathrm{d}y$(pb)	288	230	159	95	31
Stat. unc. (%)	4.3	4.4	4.8	5.7	8.5
Syst. unc. (%)	2.6	2.6	2.6	2.7	2.8
Lumi. unc. (%)	3.9	3.9	3.9	3.9	3.9

Table 2. Tabulation of numbers entering the cross-section calculation for the J/ψ analysis with statistical and systematic uncertainties for the integrated luminosity of $\mathcal{L}_{\rm tot} = 204 \pm 8\,\mathrm{pb}^{-1}$ and the fraction of single-interaction beam crossings, $\epsilon_{\rm single} = 0.3329 \pm 0.0003$.

JHEP10(2018)167

y bin	2.0−3.0	3.0−3.5	3.5−4.5
N	170	134	136
Stat. unc. (%)	7.7	8.6	8.6
$\epsilon_{\rm rec}$	0.633	0.644	0.622
Stat. unc. (%)	3.4	2.6	2.9
Syst. unc. (%)	1.3	0.6	0.6
$\epsilon_{\rm sel}$	0.650	0.664	0.671
Stat. unc. (%)	1.2	1.2	1.2
Syst. unc. (%)	1.9	1.9	1.9
Purity		0.726	
Stat. unc. (%)		8.4	
Syst. unc. (%)		1.7	
$\mathrm{d}\sigma/\mathrm{d}y$(pb)	4.4	6.6	3.4
Stat. unc. (%)	12.0	12.4	12.4
Syst. unc. (%)	2.9	2.7	2.7
Lumi. unc. (%)	3.9	3.9	3.9

Table 3. Tabulation of numbers entering the cross-section calculation for the $\psi(2S)$ analysis with statistical and systematic uncertainties for the integrated luminosity of $\mathcal{L}_{\rm tot} = 204 \pm 8\,\mathrm{pb}^{-1}$ and the fraction of single-interaction beam crossings, $\epsilon_{\rm single} = 0.3329 \pm 0.0003$.

J/ψ y bin	2.0−2.25	2.25−2.5	2.5−2.75	2.75−3.0	3.0−3.25
Acc.	0.095 ± 0.003	0.280 ± 0.005	0.460 ± 0.006	0.627 ± 0.006	0.733 ± 0.005
$\frac{\mathrm{d}\sigma}{\mathrm{d}y}$(nb)	7.76 ± 0.77	8.03 ± 0.51	7.29 ± 0.38	7.04 ± 0.33	6.78 ± 0.30
J/ψ y bin	3.25−3.50	3.50−3.75	3.75−4.0	4.0−4.25	4.25−4.5
Acc.	0.721 ± 0.005	0.620 ± 0.006	0.471 ± 0.006	0.287 ± 0.006	0.094 ± 0.004
$\frac{\mathrm{d}\sigma}{\mathrm{d}y}$(nb)	6.70 ± 0.29	6.22 ± 0.28	5.66 ± 0.29	5.55 ± 0.34	5.46 ± 0.52

$\psi(2S)$ y bin	2.0−3.0	3.0−3.5	3.5−4.5
Acc.	0.362 ± 0.003	0.726 ± 0.004	0.372 ± 0.003
$\frac{\mathrm{d}\sigma}{\mathrm{d}y}$(nb)	1.53 ± 0.25	1.16 ± 0.19	1.17 ± 0.20

Table 4. Tabulation, in bins of meson rapidity, of the fraction of decays with both muons in the range $2.0 < \eta < 4.5$ and the differential cross-sections for J/ψ and $\psi(2S)$ production calculated without fiducial requirements on the muons.

As a cross-check and to confirm the improvements brought by HERSCHEL, the cross-sections have been recalculated without imposing the HERSCHEL veto: consistent results are obtained but with a larger systematic uncertainty of about 8%. While the extracted signal contribution is comparable to figure 4 and well described by a single exponential function with a consistent value of $b_{\rm sig} = 5.92 \pm 0.06\,\mathrm{GeV}^{-2}$, the extracted proton-dissociation component requires two exponential functions to describe the distribution.

JHEP10(2018)167

To compare with theoretical predictions, which are generally expressed without fiducial requirements on the muons, the differential cross-sections for J/ψ and $\psi(2S)$ mesons as functions of the meson rapidity are calculated by correcting for the branching fractions to muon pairs, $\mathcal{B}(J/\psi \to \mu^+\mu^-) = (5.961 \pm 0.033)\%$ and $\mathcal{B}(\psi(2S) \to \mu^+\mu^-) = (0.79 \pm 0.09)\%$ [25], and for the fraction of those muons that fall inside the fiducial acceptance of the measurement. The fiducial acceptance is determined using SuperCHIC [19] assuming that the polarisation of the meson is the same as that of the photon. The acceptance values in bins of meson rapidity are tabulated in table 4 along with the differential cross-section results. These are plotted in figure 5 and compared to the theoretical calculations of refs. [28, 29]. Both measurements are in better agreement with the next-to-LO (NLO) predictions. The χ^2/ndf for the J/ψ analysis is 8.1/10 while for the $\psi(2S)$ analysis, it is 3.0/3. They are less consistent with the LO predictions having 28.5/10 and 11.0/3 for the J/ψ and $\psi(2S)$ analysis, respectively.

The cross-section for the CEP of vector mesons in pp collisions is related to the photoproduction cross-section, $\sigma_{\gamma p\to\psi p}$ [28],

$$\sigma_{pp\to p\psi p} = r(W_+)k_+\frac{\mathrm{d}n}{\mathrm{d}k_+}\sigma_{\gamma p\to\psi p}(W_+) + r(W_-)k_-\frac{\mathrm{d}n}{\mathrm{d}k_-}\sigma_{\gamma p\to\psi p}(W_-). \tag{6.1}$$

Here, r is the gap survival factor, $k_\pm \equiv M_\psi/2e^{\pm y}$ is the photon energy, $\mathrm{d}n/\mathrm{d}k_\pm$ is the photon flux and $W_\pm^2 = 2k_\pm\sqrt{s}$ is the invariant mass of the photon-proton system. Equation (6.1) shows that there is a two-fold ambiguity with W_+, W_- both contributing to one LHCb rapidity bin. Since the W_- solution contributes about one third and as it has been previously measured at HERA, this term is fixed using the H1 parametrisation of their results [5]: $\sigma_{\gamma p\to J/\psi p} = a(W/90\,\mathrm{GeV})^\delta$ with $a = 81 \pm 3$ pb and $\delta = 0.67 \pm 0.03$. For the $\psi(2S)$ W_- solution, the H1 J/ψ parametrisation is scaled by 0.166, their measured ratio of $\psi(2S)$ to J/ψ cross-sections [8]. The photon flux is taken from ref. [30] and the gap survival probabilities are taken from ref. [31]. With these inputs, which for ease of calculation are reproduced in tables 7 and 8 in the appendix, eq. (6.1) allows the calculation of $\sigma_{\gamma p\to\psi p}$ at high values of W beyond the kinematic reach of HERA.

The photoproduction cross-sections for J/ψ and $\psi(2S)$ are shown in figure 6. It includes a comparison to H1 [5], ZEUS [7] and ALICE [10] results, and at lower W values fixed target data from E401 [2], E516 [3] and E687 [4]. Also shown are previous LHCb results at $\sqrt{s} = 7\,\mathrm{TeV}$, recalculated using improved photon flux and gap survival factors. The 13 TeV LHCb data are in agreement with the 7 TeV results in the kinematic region where they overlap. However, the 13 TeV data extends the W reach to almost 2 TeV. Figure 6 also shows the power-law fit to H1 data [5] and it can be seen that this is insufficient to describe the J/ψ data at the highest energies. In contrast, the data is in good agreement with the JMRT prediction, which takes account of most of the NLO QCD effects [31] and deviates from a simple power-law shape at high W.

7 Conclusions

Measurements are presented of the cross-sections times branching fractions for exclusive J/ψ and $\psi(2S)$ mesons decaying to muons with pseudorapidities between 2.0 and 4.5. The

JHEP10(2018)167

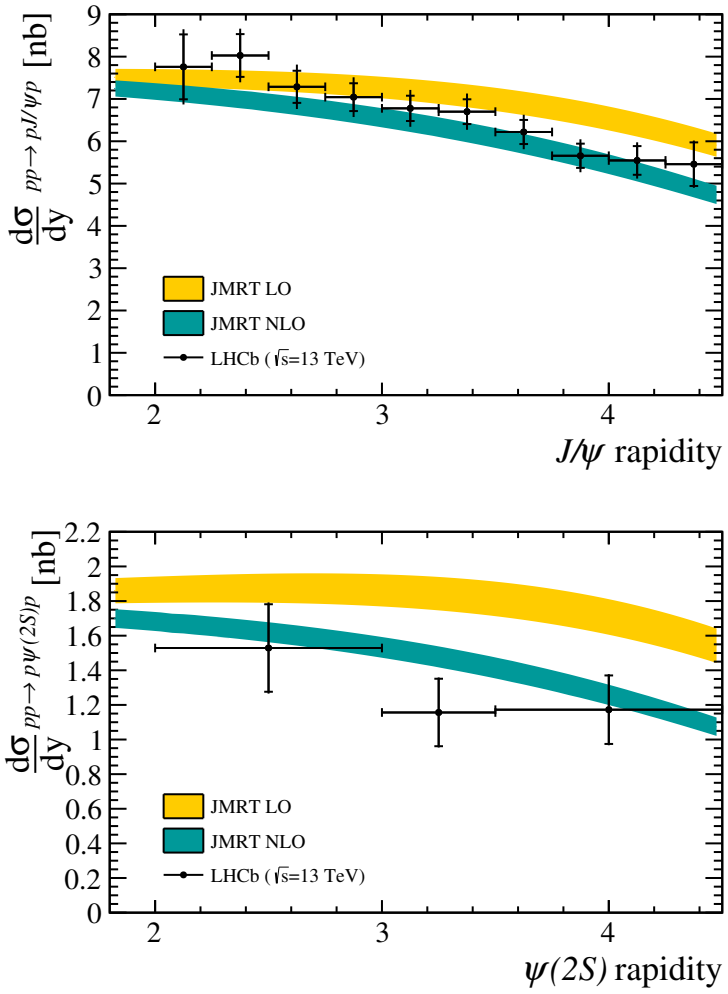

Figure 5. Differential cross-sections compared to LO and NLO theory JMRT predictions [28, 29] for the J/ψ meson (top) and the $\psi(2S)$ meson (bottom). The inner error bar represents the statistical uncertainty; the outer is the total uncertainty. Since the systematic uncertainty for the $\psi(2S)$ meson is negligible with respect to the statistical uncertainty, it is almost not visible in the lower figure.

addition of new scintillators in the forward region has resulted in lower backgrounds in pp collisions at a centre-of-mass energy $\sqrt{s} = 13\,\text{TeV}$ compared to the previous measurement at $\sqrt{s} = 7\,\text{TeV}$. As a consequence, the systematic uncertainty on the J/ψ cross-section is reduced from 5.6% at $\sqrt{s} = 7\,\text{TeV}$ to 2.7% at $\sqrt{s} = 13\,\text{TeV}$, reflecting an improved understanding of the background proton-dissociation process. After correcting for the muon acceptance, the cross-sections for the J/ψ and $\psi(2S)$ mesons are compared to theory and found to be in better agreement with the JMRT NLO rather than LO predictions. The derived cross-section for J/ψ photoproduction shows a deviation from a pure power-law extrapolation of H1 data, while the $\psi(2S)$ results are consistent although more data are required in this channel to make a critical comparison.

JHEP10(2018)167

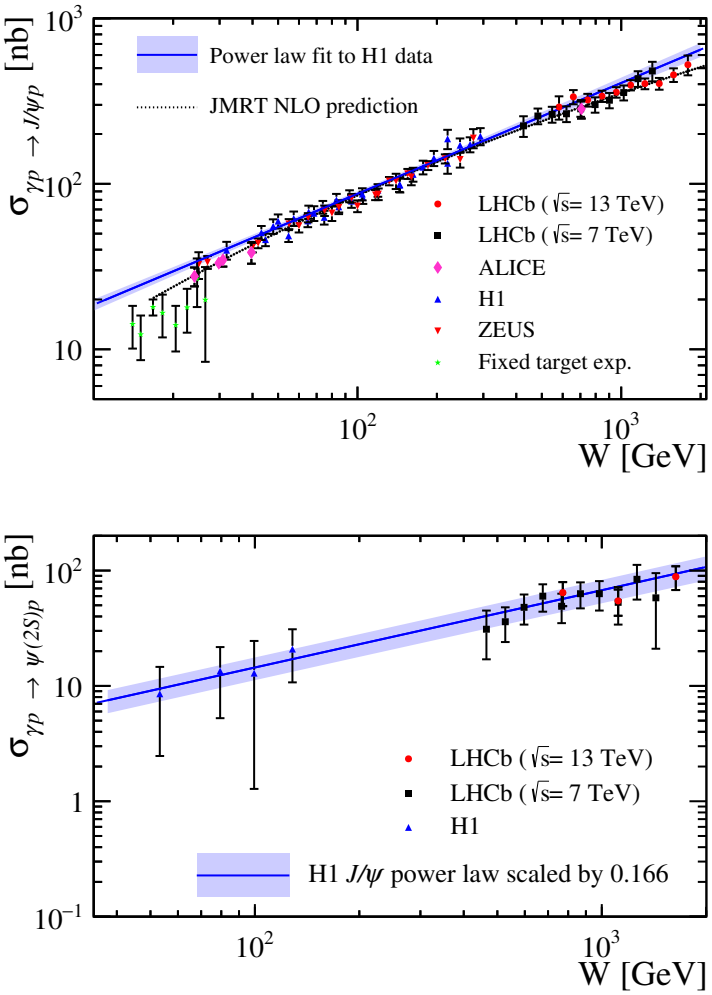

Figure 6. Compilation of photoproduction cross-sections for various experiments. The upper (lower) plot uses the J/ψ ($\psi(2S)$) data.

Acknowledgments

We express our gratitude to our colleagues in the CERN accelerator departments for the excellent performance of the LHC. We thank the technical and administrative staff at the LHCb institutes. We acknowledge support from CERN and from the national agencies: CAPES, CNPq, FAPERJ and FINEP (Brazil); MOST and NSFC (China); CNRS/IN2P3 (France); BMBF, DFG and MPG (Germany); INFN (Italy); NWO (Netherlands); MNiSW and NCN (Poland); MEN/IFA (Romania); MinES and FASO (Russia); MinECo (Spain); SNSF and SER (Switzerland); NASU (Ukraine); STFC (United Kingdom); NSF (U.S.A.). We acknowledge the computing resources that are provided by CERN, IN2P3 (France), KIT and DESY (Germany), INFN (Italy), SURF (Netherlands), PIC (Spain), GridPP (United Kingdom), RRCKI and Yandex LLC (Russia), CSCS (Switzerland), IFIN-HH (Romania), CBPF (Brazil), PL-GRID (Poland) and OSC (U.S.A.). We are indebted to the communities behind the multiple open-source software packages on which we depend. Individual groups

JHEP10(2018)167

or members have received support from AvH Foundation (Germany), EPLANET, Marie Skłodowska-Curie Actions and ERC (European Union), ANR, Labex P2IO and OCEVU, and Région Auvergne-Rhône-Alpes (France), Key Research Program of Frontier Sciences of CAS, CAS PIFI, and the Thousand Talents Program (China), RFBR, RSF and Yandex LLC (Russia), GVA, XuntaGal and GENCAT (Spain), Herchel Smith Fund, the Royal Society, the English-Speaking Union and the Leverhulme Trust (United Kingdom).

A Additional material

1.00	0.58	0.58	0.57	0.57	0.57	0.56	0.54	0.51	0.40
	1.00	0.71	0.71	0.71	0.71	0.70	0.67	0.62	0.49
		1.00	0.74	0.74	0.74	0.73	0.69	0.64	0.50
			1.00	0.76	0.75	0.74	0.71	0.65	0.50
				1.00	0.76	0.74	0.71	0.65	0.50
					1.00	0.74	0.71	0.65	0.50
						1.00	0.69	0.64	0.49
							1.00	0.61	0.46
								1.00	0.43
									1.00

1.00	0.74	0.88	0.78	0.68	0.69	0.71	0.64	0.77	0.76
	1.00	0.91	0.96	0.95	0.95	0.96	0.94	0.96	0.93
		1.00	0.94	0.88	0.89	0.91	0.86	0.94	0.92
			1.00	0.97	0.97	0.98	0.95	0.98	0.95
				1.00	0.99	0.99	0.99	0.97	0.93
					1.00	0.99	0.98	0.98	0.94
						1.00	0.99	0.99	0.95
							1.00	0.97	0.93
								1.00	0.96
									1.00

Table 5. (Top) Statistical and (bottom) systematic correlation matrices for J/ψ, where each column corresponds to one rapidity bin in increasing order. As the matrix is symmetric, only the top triangle is shown.

1.00	0.55	0.56
	1.00	0.52
		1.00

1.00	0.95	0.96
	1.00	1.00
		1.00

Table 6. (Top) Statistical and (bottom) systematic correlation matrices for $\psi(2S)$, where each column corresponds to one rapidity bin in increasing order. As the matrix is symmetric, only the top triangle is shown.

JHEP10(2018)167

J/ψ y bin	2.0−2.25	2.25−2.5	2.5−2.75	2.75−3.0	3.0−3.25
W_+ (GeV)	581	658	746	845	958
$k_+ \mathrm{d}n/\mathrm{d}k_+ (\times 10^{-3})$	22.7	21.6	20.4	19.2	18.0
$r(W_+)$	0.786	0.774	0.762	0.748	0.732
W_- (GeV)	69.4	61.2	54.0	47.7	42.1
$k_- \mathrm{d}n/\mathrm{d}k_- (\times 10^{-3})$	42.5	43.7	44.9	46.0	47.2
$r(W_-)$	0.885	0.888	0.891	0.893	0.896
$\sigma_{\gamma p \to J/\psi p(W_-)}$ (nb)					
Power law	68.0	62.6	57.6	52.9	48.7
JMRT NLO	65.3	59.5	54.1	49.1	44.5
Calculated:					
$\sigma_{\gamma p \to J/\psi p(W_+)}$ (nb)					
Power law	291	335	321	339	358
JMRT NLO	297	343	330	350	371

J/ψ y bin	3.25−3.50	3.50−3.75	3.75−4.0	4.0−4.25	4.25−4.5
W_+ (GeV)	1085	1230	1394	1579	1790
$k_+ \mathrm{d}n/\mathrm{d}k_+ (\times 10^{-3})$	16.8	15.7	14.5	13.3	12.1
$r(W_+)$	0.715	0.695	0.672	0.647	0.618
W_- (GeV)	37.1	32.8	28.9	25.5	22.5
$k_- \mathrm{d}n/\mathrm{d}k_- (\times 10^{-3})$	48.3	49.5	50.7	51.8	53.0
$r(W_-)$	0.898	0.901	0.903	0.905	0.907
$\sigma_{\gamma p \to J/\psi p(W_-)}$ (nb)					
Power law	44.8	41.2	37.9	34.8	32.0
JMRT NLO	40.2	36.3	32.7	29.5	26.4
Calculated:					
$\sigma_{\gamma p \to J/\psi p(W_+)}$ (nb)					
Power law	395	403	403	456	524
JMRT NLO	411	423	427	485	560

$\psi(2S)$ y bin	2.0−3.0	3.0−3.5	3.5−4.5
W_+ (GeV)	772	1115	1634
$k_+ \mathrm{d}n/\mathrm{d}k_+ (\times 10^{-3})$	21.5	18.5	14.4
$r(W_+)$	0.787	0.762	0.677
W_- (GeV)	63.4	43.2	29.9
$k_- \mathrm{d}n/\mathrm{d}k_- (\times 10^{-3})$	45.3	49.9	52.4
$r(W_-)$	0.911	0.942	0.926
$\sigma_{\gamma p \to \psi(2S) p(W_-)}$ (nb)			
Power law	10.6	8.2	6.4
Calculated:			
$\sigma_{\gamma p \to \psi(2S) p(W_+)}$ (nb)			
Power law	64	55	88

Table 7. Values used in evaluating the photo-production cross-section using eq. (6.1) for the J/ψ and $\psi(2S)$ analysis with gap survival factors for the production of J/ψ and $\psi(2S)$ mesons at $\sqrt{s} = 13\,\mathrm{TeV}$ [31]. For the J/ψ analyis, $\sigma_{\gamma p \to J/\psi p(W_+)}$ is calculated using the power-law description of HERA or the JMRT NLO description for $\sigma_{\gamma p \to J/\psi p(W_-)}$.

JHEP10(2018)167

J/ψ y bin	2.00−2.25	2.25−2.50	2.50−2.75	2.75−3.00	3.00−3.25
$r(W_+)$	0.766	0.752	0.736	0.718	0.698
$r(W_-)$	0.882	0.885	0.888	0.891	0.894
J/ψ y bin	3.25−3.50	3.50−3.75	3.75−4.00	4.00−4.25	4.25−4.50
$r(W_+)$	0.676	0.650	0.620	0.587	0.550
$r(W_-)$	0.897	0.899	0.902	0.904	0.906
$\psi(2S)$ y bin	2.00−2.25	2.25−2.50	2.50−2.75	2.75−3.00	3.00−3.25
$r(W_+)$	0.757	0.741	0.724	0.705	0.683
$r(W_-)$	0.879	0.882	0.886	0.889	0.892
$\psi(2S)$ y bin	3.25−3.50	3.50−3.75	3.75−4.00	4.00−4.25	4.25−4.50
$r(W_+)$	0.658	0.630	0.598	0.562	0.522
$r(W_-)$	0.895	0.898	0.900	0.903	0.905

Table 8. Gap survival factors for the production of J/ψ and $\psi(2S)$ mesons at $\sqrt{s} = 7\,\text{TeV}$.

Note that the correlation in the statistical covariance matrix is due to the conversion of the statistical uncertainty on the reconstruced efficiency for each pseudorapidity bin η of the two muons to the rapidity bin y of the J/ψ or $\psi(2S)$.

References

[1] M.G. Albrow, T.D. Coughlin and J.R. Forshaw, *Central exclusive particle production at high energy hadron colliders*, *Prog. Part. Nucl. Phys.* **65** (2010) 149 [arXiv:1006.1289] [INSPIRE].

[2] M.E. Binkley et al., *J/ψ photoproduction from 60 GeV/c to 300 GeV/c*, *Phys. Rev. Lett.* **48** (1982) 73 [INSPIRE].

[3] B.H. Denby et al., *Inelastic and elastic photoproduction of J/ψ(3097)*, *Phys. Rev. Lett.* **52** (1984) 795 [INSPIRE].

[4] E687 collaboration, P.L. Frabetti et al., *A measurement of elastic J/ψ photoproduction cross-section at Fermilab E687*, *Phys. Lett.* **B 316** (1993) 197 [INSPIRE].

[5] H1 collaboration, C. Alexa et al., *Elastic and proton-dissociative photoproduction of J/ψ mesons at HERA*, *Eur. Phys. J.* **C 73** (2013) 2466 [arXiv:1304.5162] [INSPIRE].

JHEP10(2018)167

[6] H1 collaboration, A. Aktas et al., *Elastic J/ψ production at HERA*, *Eur. Phys. J.* **C 46** (2006) 585 [hep-ex/0510016] [INSPIRE].

[7] ZEUS collaboration, S. Chekanov et al., *Exclusive photoproduction of J/ψ mesons at HERA*, *Eur. Phys. J.* **C 24** (2002) 345 [hep-ex/0201043] [INSPIRE].

[8] H1 collaboration, C. Adloff et al., *Diffractive photoproduction of $\psi(2S)$ mesons at HERA*, *Phys. Lett.* **B 541** (2002) 251 [hep-ex/0205107] [INSPIRE].

[9] CDF collaboration, T. Aaltonen et al., *Observation of exclusive charmonium production and $\gamma + \gamma$ to $\mu^+\mu^-$ in $p\bar{p}$ collisions at $\sqrt{s} = 1.96$ TeV*, *Phys. Rev. Lett.* **102** (2009) 242001 [arXiv:0902.1271] [INSPIRE].

[10] ALICE collaboration, *Coherent J/ψ photoproduction in ultra-peripheral Pb-Pb collisions at $\sqrt{s_{\rm NN}} = 2.76$ TeV*, *Phys. Lett.* **B 718** (2013) 1273 [arXiv:1209.3715] [INSPIRE].

[11] LHCb collaboration, *Updated measurements of exclusive J/ψ and $\psi(2S)$ production cross-sections in pp collisions at $\sqrt{s} = 7$ TeV*, *J. Phys.* **G 41** (2014) 055002 [arXiv:1401.3288] [INSPIRE].

[12] V.P. Goncalves, B.D. Moreira and F.S. Navarra, *Exclusive heavy vector meson photoproduction in hadronic collisions at the LHC: predictions of the color glass condensate model for run 2 energies*, *Phys. Rev.* **D 95** (2017) 054011 [arXiv:1612.06254] [INSPIRE].

[13] P.D.B. Collins, *An introduction to Regge theory and high energy physics*, Cambridge Monographs on Mathematical Physics, Cambridge Univ. Press, Cambridge, U.K., (2009) [INSPIRE].

[14] A. Donnachie and P.V. Landshoff, *Exclusive vector meson production at HERA*, *Phys. Lett.* **B 348** (1995) 213 [hep-ph/9411368] [INSPIRE].

[15] K. Carvalho Akiba et al., *The HeRSCheL detector: high-rapidity shower counters for LHCb*, 2018 *JINST* **13** P04017 [arXiv:1801.04281] [INSPIRE].

[16] LHCb collaboration, *The LHCb detector at the LHC*, 2008 *JINST* **3** S08005 [INSPIRE].

[17] LHCb collaboration, *LHCb detector performance*, *Int. J. Mod. Phys.* **A 30** (2015) 1530022 [arXiv:1412.6352] [INSPIRE].

[18] A.A. Alves Jr. et al., *Performance of the LHCb muon system*, 2013 *JINST* **8** P02022 [arXiv:1211.1346] [INSPIRE].

[19] L.A. Harland-Lang, V.A. Khoze and M.G. Ryskin, *Exclusive physics at the LHC with SuperChic 2*, *Eur. Phys. J.* **C 76** (2016) 9 [arXiv:1508.02718] [INSPIRE].

[20] T. Sjöstrand, S. Mrenna and P.Z. Skands, *PYTHIA 6.4 physics and manual*, *JHEP* **05** (2006) 026 [hep-ph/0603175] [INSPIRE].

[21] J.A.M. Vermaseren, *Two photon processes at very high-energies*, *Nucl. Phys.* **B 229** (1983) 347 [INSPIRE].

[22] GEANT4 collaboration, J. Allison et al., *GEANT4 developments and applications*, *IEEE Trans. Nucl. Sci.* **53** (2006) 270 [INSPIRE].

[23] GEANT4 collaboration, S. Agostinelli et al., *GEANT4: a simulation toolkit*, *Nucl. Instrum. Meth.* **A 506** (2003) 250 [INSPIRE].

[24] LHCb collaboration, *The LHCb simulation application, Gauss: design, evolution and experience*, *J. Phys. Conf. Ser.* **331** (2011) 032023 [INSPIRE].

JHEP10(2018)167

[25] Particle Data Group collaboration, C. Patrignani et al., *Review of particle physics*, *Chin. Phys.* **C 40** (2016) 100001 [INSPIRE].

[26] T. Skwarnicki, *A study of the radiative cascade transitions between the Upsilon-prime and Upsilon resonances*, Ph.D. thesis, Institute of Nuclear Physics, Krakow, Poland, (1986) [INSPIRE].

[27] LHCb collaboration, *Precision luminosity measurements at LHCb*, 2014 *JINST* **9** P12005 [arXiv:1410.0149] [INSPIRE].

[28] S.P. Jones, A.D. Martin, M.G. Ryskin and T. Teubner, *Probes of the small x gluon via exclusive J/ψ and Υ production at HERA and the LHC*, *JHEP* **11** (2013) 085 [arXiv:1307.7099] [INSPIRE].

[29] S.P. Jones, A.D. Martin, M.G. Ryskin and T. Teubner, *Predictions of exclusive $\psi(2S)$ production at the LHC*, *J. Phys.* **G 41** (2014) 055009 [arXiv:1312.6795] [INSPIRE].

[30] O. Kepka, *QCD and diffraction in the ATLAS experiment at the LHC*, Ph.D. thesis, Institute of Physics of the Academy of Sciences, Prague, Czech Republic and Particle Physics Division, CEA, Saclay, France, (2009) [INSPIRE].

[31] S.P. Jones, A.D. Martin, M.G. Ryskin and T. Teubner, *Exclusive J/ψ production at the LHC in the k_T factorization approach*, *J. Phys.* **G 44** (2017) 03LT01 [arXiv:1611.03711] [INSPIRE].

JHEP10(2018)167

The LHCb collaboration

R. Aaij[27], B. Adeva[41], M. Adinolfi[48], C.A. Aidala[73], Z. Ajaltouni[5], S. Akar[59], P. Albicocco[18], J. Albrecht[10], F. Alessio[42], M. Alexander[53], A. Alfonso Albero[40], S. Ali[27], G. Alkhazov[33], P. Alvarez Cartelle[55], A.A. Alves Jr[59], S. Amato[2], S. Amerio[23], Y. Amhis[7], L. An[3], L. Anderlini[17], G. Andreassi[43], M. Andreotti[16,g], J.E. Andrews[60], R.B. Appleby[56], F. Archilli[27], P. d'Argent[12], J. Arnau Romeu[6], A. Artamonov[39], M. Artuso[61], K. Arzymatov[37], E. Aslanides[6], M. Atzeni[44], S. Bachmann[12], J.J. Back[50], S. Baker[55], V. Balagura[7,b], W. Baldini[16], A. Baranov[37], R.J. Barlow[56], S. Barsuk[7], W. Barter[56], F. Baryshnikov[70], V. Batozskaya[31], B. Batsukh[61], V. Battista[43], A. Bay[43], J. Beddow[53], F. Bedeschi[24], I. Bediaga[1], A. Beiter[61], L.J. Bel[27], N. Beliy[63], V. Bellee[43], N. Belloli[20,i], K. Belous[39], I. Belyaev[34,42], E. Ben-Haim[8], G. Bencivenni[18], S. Benson[27], S. Beranek[9], A. Berezhnoy[35], R. Bernet[44], D. Berninghoff[12], E. Bertholet[8], A. Bertolin[23], C. Betancourt[44], F. Betti[15,42], M.O. Bettler[49], M. van Beuzekom[27], Ia. Bezshyiko[44], S. Bifani[47], P. Billoir[8], A. Birnkraut[10], A. Bizzeti[17,u], M. Bjørn[57], T. Blake[50], F. Blanc[43], S. Blusk[61], D. Bobulska[53], V. Bocci[26], O. Boente Garcia[41], T. Boettcher[58], A. Bondar[38,w], N. Bondar[33], S. Borghi[56,42], M. Borisyak[37], M. Borsato[41,42], F. Bossu[7], M. Boubdir[9], T.J.V. Bowcock[54], C. Bozzi[16,42], S. Braun[12], M. Brodski[42], J. Brodzicka[29], D. Brundu[22], E. Buchanan[48], A. Buonaura[44], C. Burr[56], A. Bursche[22], J. Buytaert[42], W. Byczynski[42], S. Cadeddu[22], H. Cai[64], R. Calabrese[16,g], R. Calladine[47], M. Calvi[20,i], M. Calvo Gomez[40,m], A. Camboni[40,m], P. Campana[18], D.H. Campora Perez[42], L. Capriotti[56], A. Carbone[15,e], G. Carboni[25], R. Cardinale[19,h], A. Cardini[22], P. Carniti[20,i], L. Carson[52], K. Carvalho Akiba[2], G. Casse[54], L. Cassina[20], M. Cattaneo[42], G. Cavallero[19,h], R. Cenci[24,p], D. Chamont[7], M.G. Chapman[48], M. Charles[8], Ph. Charpentier[42], G. Chatzikonstantinidis[47], M. Chefdeville[4], V. Chekalina[37], C. Chen[3], S. Chen[22], S.-G. Chitic[42], V. Chobanova[41], M. Chrzaszcz[42], A. Chubykin[33], P. Ciambrone[18], X. Cid Vidal[41], G. Ciezarek[42], P.E.L. Clarke[52], M. Clemencic[42], H.V. Cliff[49], J. Closier[42], V. Coco[42], J. Cogan[6], E. Cogneras[5], L. Cojocariu[32], P. Collins[42], T. Colombo[42], A. Comerma-Montells[12], A. Contu[22], G. Coombs[42], S. Coquereau[40], G. Corti[42], M. Corvo[16,g], C.M. Costa Sobral[50], B. Couturier[42], G.A. Cowan[52], D.C. Craik[58], A. Crocombe[50], M. Cruz Torres[1], R. Currie[52], C. D'Ambrosio[42], F. Da Cunha Marinho[2], C.L. Da Silva[74], E. Dall'Occo[27], J. Dalseno[48], A. Danilina[34], A. Davis[3], O. De Aguiar Francisco[42], K. De Bruyn[42], S. De Capua[56], M. De Cian[43], J.M. De Miranda[1], L. De Paula[2], M. De Serio[14,d], P. De Simone[18], C.T. Dean[53], D. Decamp[4], L. Del Buono[8], B. Delaney[49], H.-P. Dembinski[11], M. Demmer[10], A. Dendek[30], D. Derkach[37], O. Deschamps[5], F. Dettori[54], B. Dey[65], A. Di Canto[42], P. Di Nezza[18], S. Didenko[70], H. Dijkstra[42], F. Dordei[42], M. Dorigo[42,y], A. Dosil Suárez[41], L. Douglas[53], A. Dovbnya[45], K. Dreimanis[54], L. Dufour[27], G. Dujany[8], P. Durante[42], J.M. Durham[74], D. Dutta[56], R. Dzhelyadin[39], M. Dziewiecki[12], A. Dziurda[42], A. Dzyuba[33], S. Easo[51], U. Egede[55], V. Egorychev[34], S. Eidelman[38,w], S. Eisenhardt[52], U. Eitschberger[10], R. Ekelhof[10], L. Eklund[53], S. Ely[61], A. Ene[32], S. Escher[9], S. Esen[27], H.M. Evans[49], T. Evans[57], A. Falabella[15], N. Farley[47], S. Farry[54], D. Fazzini[20,42,i], L. Federici[25], G. Fernandez[40], P. Fernandez Declara[42], A. Fernandez Prieto[41], F. Ferrari[15], L. Ferreira Lopes[43], F. Ferreira Rodrigues[2], M. Ferro-Luzzi[42], S. Filippov[36], R.A. Fini[14], M. Fiorini[16,g], M. Firlej[30], C. Fitzpatrick[43], T. Fiutowski[30], F. Fleuret[7,b], M. Fontana[22,42], F. Fontanelli[19,h], R. Forty[42], V. Franco Lima[54], M. Frank[42], C. Frei[42], J. Fu[21,q], W. Funk[42], C. Färber[42], M. Féo Pereira Rivello Carvalho[27], E. Gabriel[52], A. Gallas Torreira[41], D. Galli[15,e], S. Gallorini[23], S. Gambetta[52], M. Gandelman[2], P. Gandini[21], Y. Gao[3], L.M. Garcia Martin[72], B. Garcia Plana[41], J. García Pardiñas[44], J. Garra Tico[49], L. Garrido[40], D. Gascon[40], C. Gaspar[42], L. Gavardi[10], G. Gazzoni[5], D. Gerick[12], E. Gersabeck[56], M. Gersabeck[56], T. Gershon[50], Ph. Ghez[4], S. Gianì[43], V. Gibson[49], O.G. Girard[43], L. Giubega[32], K. Gizdov[52], V.V. Gligorov[8], D. Golubkov[34], A. Golutvin[55,70], A. Gomes[1,a], I.V. Gorelov[35],

JHEP10(2018)167

C. Gotti[20,i], E. Govorkova[27], J.P. Grabowski[12], R. Graciani Diaz[40], L.A. Granado Cardoso[42], E. Graugés[40], E. Graverini[44], G. Graziani[17], A. Grecu[32], R. Greim[27], P. Griffith[22], L. Grillo[56], L. Gruber[42], B.R. Gruberg Cazon[57], O. Grünberg[67], C. Gu[3], E. Gushchin[36], Yu. Guz[39,42], T. Gys[42], C. Göbel[62], T. Hadavizadeh[57], C. Hadjivasiliou[5], G. Haefeli[43], C. Haen[42], S.C. Haines[49], B. Hamilton[60], X. Han[12], T.H. Hancock[57], S. Hansmann-Menzemer[12], N. Harnew[57], S.T. Harnew[48], C. Hasse[42], M. Hatch[42], J. He[63], M. Hecker[55], K. Heinicke[10], A. Heister[9], K. Hennessy[54], L. Henry[72], E. van Herwijnen[42], M. Heß[67], A. Hicheur[2], D. Hill[57], M. Hilton[56], P.H. Hopchev[43], W. Hu[65], W. Huang[63], Z.C. Huard[59], W. Hulsbergen[27], T. Humair[55], M. Hushchyn[37], D. Hutchcroft[54], D. Hynds[27], P. Ibis[10], M. Idzik[30], P. Ilten[47], K. Ivshin[33], R. Jacobsson[42], J. Jalocha[57], E. Jans[27], A. Jawahery[60], F. Jiang[3], M. John[57], D. Johnson[42], C.R. Jones[49], C. Joram[42], B. Jost[42], N. Jurik[57], S. Kandybei[45], M. Karacson[42], J.M. Kariuki[48], S. Karodia[53], N. Kazeev[37], M. Kecke[12], F. Keizer[49], M. Kelsey[61], M. Kenzie[49], T. Ketel[28], E. Khairullin[37], B. Khanji[12], C. Khurewathanakul[43], K.E. Kim[61], T. Kirn[9], S. Klaver[18], K. Klimaszewski[31], T. Klimkovich[11], S. Koliiev[46], M. Kolpin[12], R. Kopecna[12], P. Koppenburg[27], S. Kotriakhova[33], M. Kozeiha[5], L. Kravchuk[36], M. Kreps[50], F. Kress[55], P. Krokovny[38,w], W. Krupa[30], W. Krzemien[31], W. Kucewicz[29,l], M. Kucharczyk[29], V. Kudryavtsev[38,w], A.K. Kuonen[43], T. Kvaratskheliya[34,42], D. Lacarrere[42], G. Lafferty[56], A. Lai[22], D. Lancierini[44], G. Lanfranchi[18], C. Langenbruch[9], T. Latham[50], C. Lazzeroni[47], R. Le Gac[6], A. Leflat[35], J. Lefrançois[7], R. Lefèvre[5], F. Lemaitre[42], O. Leroy[6], T. Lesiak[29], B. Leverington[12], P.-R. Li[63], T. Li[3], Z. Li[61], X. Liang[61], T. Likhomanenko[69], R. Lindner[42], F. Lionetto[44], V. Lisovskyi[7], X. Liu[3], D. Loh[50], A. Loi[22], I. Longstaff[53], J.H. Lopes[2], D. Lucchesi[23,o], M. Lucio Martinez[41], A. Lupato[23], E. Luppi[16,g], O. Lupton[42], A. Lusiani[24], X. Lyu[63], F. Machefert[7], F. Maciuc[32], V. Macko[43], P. Mackowiak[10], S. Maddrell-Mander[48], O. Maev[33,42], K. Maguire[56], D. Maisuzenko[33], M.W. Majewski[30], S. Malde[57], B. Malecki[29], A. Malinin[69], T. Maltsev[38,w], G. Manca[22,f], G. Mancinelli[6], D. Marangotto[21,q], J. Maratas[5,v], J.F. Marchand[4], U. Marconi[15], C. Marin Benito[40], M. Marinangeli[43], P. Marino[43], J. Marks[12], G. Martellotti[26], M. Martin[6], M. Martinelli[43], D. Martinez Santos[41], F. Martinez Vidal[72], A. Massafferri[1], R. Matev[42], A. Mathad[50], Z. Mathe[42], C. Matteuzzi[20], A. Mauri[44], E. Maurice[7,b], B. Maurin[43], A. Mazurov[47], M. McCann[55,42], A. McNab[56], R. McNulty[13], J.V. Mead[54], B. Meadows[59], C. Meaux[6], F. Meier[10], N. Meinert[67], D. Melnychuk[31], M. Merk[27], A. Merli[21,q], E. Michielin[23], D.A. Milanes[66], E. Millard[50], M.-N. Minard[4], L. Minzoni[16,g], D.S. Mitzel[12], A. Mogini[8], J. Molina Rodriguez[1,z], T. Mombächer[10], I.A. Monroy[66], S. Monteil[5], M. Morandin[23], G. Morello[18], M.J. Morello[24,t], O. Morgunova[69], J. Moron[30], A.B. Morris[6], R. Mountain[61], F. Muheim[52], M. Mulder[27], D. Müller[42], J. Müller[10], K. Müller[44], V. Müller[10], P. Naik[48], T. Nakada[43], R. Nandakumar[51], A. Nandi[57], T. Nanut[43], I. Nasteva[2], M. Needham[52], N. Neri[21], S. Neubert[12], N. Neufeld[42], M. Neuner[12], T.D. Nguyen[43], C. Nguyen-Mau[43,n], S. Nieswand[9], R. Niet[10], N. Nikitin[35], A. Nogay[69], D.P. O'Hanlon[15], A. Oblakowska-Mucha[30], V. Obraztsov[39], S. Ogilvy[18], R. Oldeman[22,f], C.J.G. Onderwater[68], A. Ossowska[29], J.M. Otalora Goicochea[2], P. Owen[44], A. Oyanguren[72], P.R. Pais[43], A. Palano[14], M. Palutan[18,42], G. Panshin[71], A. Papanestis[51], M. Pappagallo[52], L.L. Pappalardo[16,g], W. Parker[60], C. Parkes[56], G. Passaleva[17,42], A. Pastore[14], M. Patel[55], C. Patrignani[15,e], A. Pearce[42], A. Pellegrino[27], G. Penso[26], M. Pepe Altarelli[42], S. Perazzini[42], D. Pereima[34], P. Perret[5], L. Pescatore[43], K. Petridis[48], A. Petrolini[19,h], A. Petrov[69], M. Petruzzo[21,q], B. Pietrzyk[4], G. Pietrzyk[43], M. Pikies[29], D. Pinci[26], J. Pinzino[42], F. Pisani[42], A. Pistone[19,h], A. Piucci[12], V. Placinta[32], S. Playfer[52], J. Plews[47], M. Plo Casasus[41], F. Polci[8], M. Poli Lener[18], A. Poluektov[50], N. Polukhina[70,c], I. Polyakov[61], E. Polycarpo[2], G.J. Pomery[48], S. Ponce[42], A. Popov[39], D. Popov[47,11], S. Poslavskii[39], C. Potterat[2], E. Price[48], J. Prisciandaro[41], C. Prouve[48], V. Pugatch[46], A. Puig Navarro[44], H. Pullen[57], G. Punzi[24,p], W. Qian[63], J. Qin[63], R. Quagliani[8], B. Quintana[5], B. Rachwal[30], J.H. Rademacker[48], M. Rama[24],

JHEP10(2018)167

M. Ramos Pernas[41], M.S. Rangel[2], F. Ratnikov[37,x], G. Raven[28], M. Ravonel Salzgeber[42], M. Reboud[4], F. Redi[43], S. Reichert[10], A.C. dos Reis[1], F. Reiss[8], C. Remon Alepuz[72], Z. Ren[3], V. Renaudin[7], S. Ricciardi[51], S. Richards[48], K. Rinnert[54], P. Robbe[7], A. Robert[8], A.B. Rodrigues[43], E. Rodrigues[59], J.A. Rodriguez Lopez[66], A. Rogozhnikov[37], S. Roiser[42], A. Rollings[57], V. Romanovskiy[39], A. Romero Vidal[41], M. Rotondo[18], M.S. Rudolph[61], T. Ruf[42], J. Ruiz Vidal[72], J.J. Saborido Silva[41], N. Sagidova[33], B. Saitta[22,f], V. Salustino Guimaraes[62], C. Sanchez Gras[27], C. Sanchez Mayordomo[72], B. Sanmartin Sedes[41], R. Santacesaria[26], C. Santamarina Rios[41], M. Santimaria[18], E. Santovetti[25,j], G. Sarpis[56], A. Sarti[18,k], C. Satriano[26,s], A. Satta[25], M. Saur[63], D. Savrina[34,35], S. Schael[9], M. Schellenberg[10], M. Schiller[53], H. Schindler[42], M. Schmelling[11], T. Schmelzer[10], B. Schmidt[42], O. Schneider[43], A. Schopper[42], H.F. Schreiner[59], M. Schubiger[43], M.H. Schune[7], R. Schwemmer[42], B. Sciascia[18], A. Sciubba[26,k], A. Semennikov[34], E.S. Sepulveda[8], A. Sergi[47,42], N. Serra[44], J. Serrano[6], L. Sestini[23], P. Seyfert[42], M. Shapkin[39], Y. Shcheglov[33,†], T. Shears[54], L. Shekhtman[38,w], V. Shevchenko[69], E. Shmanin[70], B.G. Siddi[16], R. Silva Coutinho[44], L. Silva de Oliveira[2], G. Simi[23,o], S. Simone[14,d], N. Skidmore[12], T. Skwarnicki[61], E. Smith[9], I.T. Smith[52], M. Smith[55], M. Soares[15], l. Soares Lavra[1], M.D. Sokoloff[59], F.J.P. Soler[53], B. Souza De Paula[2], B. Spaan[10], P. Spradlin[53], F. Stagni[42], M. Stahl[12], S. Stahl[42], P. Stefko[43], S. Stefkova[55], O. Steinkamp[44], S. Stemmle[12], O. Stenyakin[39], M. Stepanova[33], H. Stevens[10], S. Stone[61], B. Storaci[44], S. Stracka[24,p], M.E. Stramaglia[43], M. Straticiuc[32], U. Straumann[44], S. Strokov[71], J. Sun[3], L. Sun[64], K. Swientek[30], V. Syropoulos[28], T. Szumlak[30], M. Szymanski[63], S. T'Jampens[4], Z. Tang[3], A. Tayduganov[6], T. Tekampe[10], G. Tellarini[16], F. Teubert[42], E. Thomas[42], J. van Tilburg[27], M.J. Tilley[55], V. Tisserand[5], M. Tobin[43], S. Tolk[42], L. Tomassetti[16,g], D. Tonelli[24], D.Y. Tou[8], R. Tourinho Jadallah Aoude[1], E. Tournefier[4], M. Traill[53], M.T. Tran[43], A. Trisovic[49], A. Tsaregorodtsev[6], A. Tully[49], N. Tuning[27,42], A. Ukleja[31], A. Usachov[7], A. Ustyuzhanin[37], U. Uwer[12], C. Vacca[22,f], A. Vagner[71], V. Vagnoni[15], A. Valassi[42], S. Valat[42], G. Valenti[15], R. Vazquez Gomez[42], P. Vazquez Regueiro[41], S. Vecchi[16], M. van Veghel[27], J.J. Velthuis[48], M. Veltri[17,r], G. Veneziano[57], A. Venkateswaran[61], T.A. Verlage[9], M. Vernet[5], M. Vesterinen[57], J.V. Viana Barbosa[42], D. Vieira[63], M. Vieites Diaz[41], H. Viemann[67], X. Vilasis-Cardona[40,m], A. Vitkovskiy[27], M. Vitti[49], V. Volkov[35], A. Vollhardt[44], B. Voneki[42], A. Vorobyev[33], V. Vorobyev[38,w], C. Voß[9], J.A. de Vries[27], C. Vázquez Sierra[27], R. Waldi[67], J. Walsh[24], J. Wang[61], M. Wang[3], Y. Wang[65], Z. Wang[44], D.R. Ward[49], H.M. Wark[54], N.K. Watson[47], D. Websdale[55], A. Weiden[44], C. Weisser[58], M. Whitehead[9], J. Wicht[50], G. Wilkinson[57], M. Wilkinson[61], M.R.J. Williams[56], M. Williams[58], T. Williams[47], F.F. Wilson[51,42], J. Wimberley[60], M. Winn[7], J. Wishahi[10], W. Wislicki[31], M. Witek[29], G. Wormser[7], S.A. Wotton[49], K. Wyllie[42], D. Xiao[65], Y. Xie[65], A. Xu[3], M. Xu[65], Q. Xu[63], Z. Xu[3], Z. Xu[4], Z. Yang[3], Z. Yang[60], Y. Yao[61], H. Yin[65], J. Yu[65,ab], X. Yuan[61], O. Yushchenko[39], K.A. Zarebski[47], M. Zavertyaev[11,c], D. Zhang[65], L. Zhang[3], W.C. Zhang[3,aa], Y. Zhang[7], A. Zhelezov[12], Y. Zheng[63], X. Zhu[3], V. Zhukov[9,35], J.B. Zonneveld[52] and S. Zucchelli[15]

[1] *Centro Brasileiro de Pesquisas Físicas (CBPF), Rio de Janeiro, Brazil*
[2] *Universidade Federal do Rio de Janeiro (UFRJ), Rio de Janeiro, Brazil*
[3] *Center for High Energy Physics, Tsinghua University, Beijing, China*
[4] *Univ. Grenoble Alpes, Univ. Savoie Mont Blanc, CNRS, IN2P3-LAPP, Annecy, France*
[5] *Clermont Université, Université Blaise Pascal, CNRS/IN2P3, LPC, Clermont-Ferrand, France*
[6] *Aix Marseille Univ, CNRS/IN2P3, CPPM, Marseille, France*
[7] *LAL, Univ. Paris-Sud, CNRS/IN2P3, Université Paris-Saclay, Orsay, France*
[8] *LPNHE, Sorbonne Université, Paris Diderot Sorbonne Paris Cité, CNRS/IN2P3, Paris, France*
[9] *I. Physikalisches Institut, RWTH Aachen University, Aachen, Germany*
[10] *Fakultät Physik, Technische Universität Dortmund, Dortmund, Germany*

JHEP10(2018)167

[11] *Max-Planck-Institut für Kernphysik (MPIK), Heidelberg, Germany*
[12] *Physikalisches Institut, Ruprecht-Karls-Universität Heidelberg, Heidelberg, Germany*
[13] *School of Physics, University College Dublin, Dublin, Ireland*
[14] *INFN Sezione di Bari, Bari, Italy*
[15] *INFN Sezione di Bologna, Bologna, Italy*
[16] *INFN Sezione di Ferrara, Ferrara, Italy*
[17] *INFN Sezione di Firenze, Firenze, Italy*
[18] *INFN Laboratori Nazionali di Frascati, Frascati, Italy*
[19] *INFN Sezione di Genova, Genova, Italy*
[20] *INFN Sezione di Milano-Bicocca, Milano, Italy*
[21] *INFN Sezione di Milano, Milano, Italy*
[22] *INFN Sezione di Cagliari, Monserrato, Italy*
[23] *INFN Sezione di Padova, Padova, Italy*
[24] *INFN Sezione di Pisa, Pisa, Italy*
[25] *INFN Sezione di Roma Tor Vergata, Roma, Italy*
[26] *INFN Sezione di Roma La Sapienza, Roma, Italy*
[27] *Nikhef National Institute for Subatomic Physics, Amsterdam, Netherlands*
[28] *Nikhef National Institute for Subatomic Physics and VU University Amsterdam, Amsterdam, Netherlands*
[29] *Henryk Niewodniczanski Institute of Nuclear Physics Polish Academy of Sciences, Kraków, Poland*
[30] *AGH - University of Science and Technology, Faculty of Physics and Applied Computer Science, Kraków, Poland*
[31] *National Center for Nuclear Research (NCBJ), Warsaw, Poland*
[32] *Horia Hulubei National Institute of Physics and Nuclear Engineering, Bucharest-Magurele, Romania*
[33] *Petersburg Nuclear Physics Institute (PNPI), Gatchina, Russia*
[34] *Institute of Theoretical and Experimental Physics (ITEP), Moscow, Russia*
[35] *Institute of Nuclear Physics, Moscow State University (SINP MSU), Moscow, Russia*
[36] *Institute for Nuclear Research of the Russian Academy of Sciences (INR RAS), Moscow, Russia*
[37] *Yandex School of Data Analysis, Moscow, Russia*
[38] *Budker Institute of Nuclear Physics (SB RAS), Novosibirsk, Russia*
[39] *Institute for High Energy Physics (IHEP), Protvino, Russia*
[40] *ICCUB, Universitat de Barcelona, Barcelona, Spain*
[41] *Instituto Galego de Física de Altas Enerxías (IGFAE), Universidade de Santiago de Compostela, Santiago de Compostela, Spain*
[42] *European Organization for Nuclear Research (CERN), Geneva, Switzerland*
[43] *Institute of Physics, Ecole Polytechnique Fédérale de Lausanne (EPFL), Lausanne, Switzerland*
[44] *Physik-Institut, Universität Zürich, Zürich, Switzerland*
[45] *NSC Kharkiv Institute of Physics and Technology (NSC KIPT), Kharkiv, Ukraine*
[46] *Institute for Nuclear Research of the National Academy of Sciences (KINR), Kyiv, Ukraine*
[47] *University of Birmingham, Birmingham, United Kingdom*
[48] *H.H. Wills Physics Laboratory, University of Bristol, Bristol, United Kingdom*
[49] *Cavendish Laboratory, University of Cambridge, Cambridge, United Kingdom*
[50] *Department of Physics, University of Warwick, Coventry, United Kingdom*
[51] *STFC Rutherford Appleton Laboratory, Didcot, United Kingdom*
[52] *School of Physics and Astronomy, University of Edinburgh, Edinburgh, United Kingdom*
[53] *School of Physics and Astronomy, University of Glasgow, Glasgow, United Kingdom*
[54] *Oliver Lodge Laboratory, University of Liverpool, Liverpool, United Kingdom*
[55] *Imperial College London, London, United Kingdom*
[56] *School of Physics and Astronomy, University of Manchester, Manchester, United Kingdom*
[57] *Department of Physics, University of Oxford, Oxford, United Kingdom*
[58] *Massachusetts Institute of Technology, Cambridge, MA, United States*

JHEP10(2018)167

[59] University of Cincinnati, Cincinnati, OH, United States
[60] University of Maryland, College Park, MD, United States
[61] Syracuse University, Syracuse, NY, United States
[62] Pontifícia Universidade Católica do Rio de Janeiro (PUC-Rio), Rio de Janeiro, Brazil, associated to [2]
[63] University of Chinese Academy of Sciences, Beijing, China, associated to [3]
[64] School of Physics and Technology, Wuhan University, Wuhan, China, associated to [3]
[65] Institute of Particle Physics, Central China Normal University, Wuhan, Hubei, China, associated to [3]
[66] Departamento de Fisica , Universidad Nacional de Colombia, Bogota, Colombia, associated to [8]
[67] Institut für Physik, Universität Rostock, Rostock, Germany, associated to [12]
[68] Van Swinderen Institute, University of Groningen, Groningen, Netherlands, associated to [27]
[69] National Research Centre Kurchatov Institute, Moscow, Russia, associated to [34]
[70] National University of Science and Technology "MISIS", Moscow, Russia, associated to [34]
[71] National Research Tomsk Polytechnic University, Tomsk, Russia, associated to [34]
[72] Instituto de Fisica Corpuscular, Centro Mixto Universidad de Valencia - CSIC, Valencia, Spain, associated to [40]
[73] University of Michigan, Ann Arbor, United States, associated to [61]
[74] Los Alamos National Laboratory (LANL), Los Alamos, United States, associated to [61]

[a] Universidade Federal do Triângulo Mineiro (UFTM), Uberaba-MG, Brazil
[b] Laboratoire Leprince-Ringuet, Palaiseau, France
[c] P.N. Lebedev Physical Institute, Russian Academy of Science (LPI RAS), Moscow, Russia
[d] Università di Bari, Bari, Italy
[e] Università di Bologna, Bologna, Italy
[f] Università di Cagliari, Cagliari, Italy
[g] Università di Ferrara, Ferrara, Italy
[h] Università di Genova, Genova, Italy
[i] Università di Milano Bicocca, Milano, Italy
[j] Università di Roma Tor Vergata, Roma, Italy
[k] Università di Roma La Sapienza, Roma, Italy
[l] AGH - University of Science and Technology, Faculty of Computer Science, Electronics and Telecommunications, Kraków, Poland
[m] LIFAELS, La Salle, Universitat Ramon Llull, Barcelona, Spain
[n] Hanoi University of Science, Hanoi, Vietnam
[o] Università di Padova, Padova, Italy
[p] Università di Pisa, Pisa, Italy
[q] Università degli Studi di Milano, Milano, Italy
[r] Università di Urbino, Urbino, Italy
[s] Università della Basilicata, Potenza, Italy
[t] Scuola Normale Superiore, Pisa, Italy
[u] Università di Modena e Reggio Emilia, Modena, Italy
[v] MSU - Iligan Institute of Technology (MSU-IIT), Iligan, Philippines
[w] Novosibirsk State University, Novosibirsk, Russia
[x] National Research University Higher School of Economics, Moscow, Russia
[y] Sezione INFN di Trieste, Trieste, Italy
[z] Escuela Agrícola Panamericana, San Antonio de Oriente, Honduras
[aa] School of Physics and Information Technology, Shaanxi Normal University (SNNU), Xi'an, China
[ab] Physics and Micro Electronic College, Hunan University, Changsha City, China
[†] Deceased

JHEP10(2018)167